Available online at www.sciencedirect.com
SCIENCE DIRECT®
Journal of Theoretical Biology 240 (2006) 1–8
Journal of Theoretical Biology
www.elsevier.com/locate/yjtbi

Biomechanical model for appressorial design in *Magnaporthe grisea*

Anthony Tongen[1], Alain Goriely, Michael Tabor*

Program in Applied Mathematics and Department of Mathematics, University of Arizona, Building #89, Tucson, AZ 85721, USA

Received 16 December 2004; received in revised form 5 July 2005; accepted 18 August 2005
Available online 3 October 2005

Abstract

The fungus *Magnaporthe grisea*, commonly referred to as the rice blast fungus, is responsible for destroying from 10% to 30% of the world's rice crop each year. The fungus attaches to the rice leaf and forms a dome-shaped structure, the appressorium, in which enormous pressures are generated that are used to blast a penetration peg through the rice cell walls and infect the plant. We develop a model of the appressorial design in terms of a bioelastic shell that can explain the shape of the appressorium, and its ability to maintain that shape under the enormous increases in turgor pressure that can occur during the penetration phase.

Keywords: Rice blast fungus; Bioelastic shell; Nonlinear elasticity

1. Introduction

Rice is one of the most important commodities worldwide for both food and barter, and the fact that each year the fungus *Magnaporthe grisea* causes losses of between 10% and 30% of the approximately 520 million metric tons of rice harvested per year (Talbot, 2003), makes this lethal microorganism an important topic of study. The commonly used term rice blast fungus is highly appropriate given that it deploys enormous turgor pressures to operate a violent "breaking and entering" mechanism to infect its host. There have been many studies of the fungus in the mycological literature that have raised interesting questions concerning the biomechanical aspects of its operation (Bastmeyer et al., 2002), and it is some of these questions that we attempt to address here.

A detailed description of all the biological processes involved is, of course, beyond the scope of this paper, but it is appropriate to give a summary of some the key steps relevant to our study. A simple cartoon of the overall process is given in Fig. 1.

1. A conidium lands on the rice leaf surface and attaches to it using material known as spore tip mucilage. Once attached, it is very hard to dislodge the conidium.
2. A germ tube grows out of the conidium, hooks into the surface of the rice leaf, and begins to form an appressorium. Experimental evidence (Money and Howard, 1996) indicates that turgor pressures of the order 3–5 atmospheres develop in the appressorium. The mechanisms by which the appressorium is initially built and the interplay with the initial turgor pressure are not well understood.
3. The germ tube is eventually shut off from the appressorium leaving the latter as a separate, independent, unit.
4. The appressorium adheres to the plant surface by means of a highly potent adhesive in a ring around its base. The inner region of contact between the appressorium and leaf surface, termed the appressorial pore, appears to lack any obvious appressorial cell wall structure.
5. A melanin layer develops within the appressorium (but not over the appressorial pore). The "melanization" process is signaled by a darkening of the appressorial wall. The melanin layer allows only water molecules to permeate the wall and, on interaction with an internal

*Corresponding author.
E-mail addresses: tongen@math.jmu.edu (A. Tongen), goriely@math.arizona.edu (A. Goriely), tabor@math.arizona.edu (M. Tabor).
URL: http://math.arizona.edu/~goriely.
[1]Current address: Department of Mathematics and Statistics, James Madison University.

0022-5193/$ - see front matter © 2005 Elsevier Ltd. All rights reserved.
doi:10.1016/j.jtbi.2005.08.014

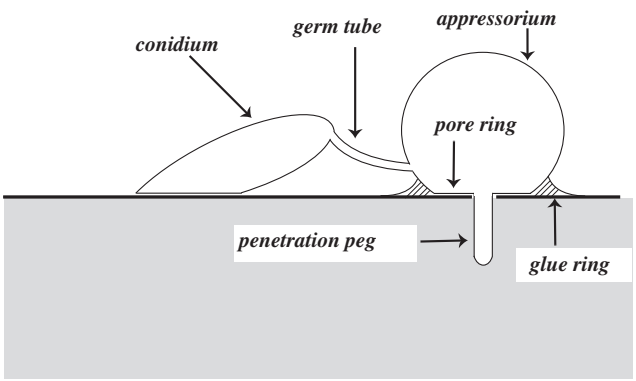

Fig. 1. Pictorial representation of the development of the rice blast fungus.

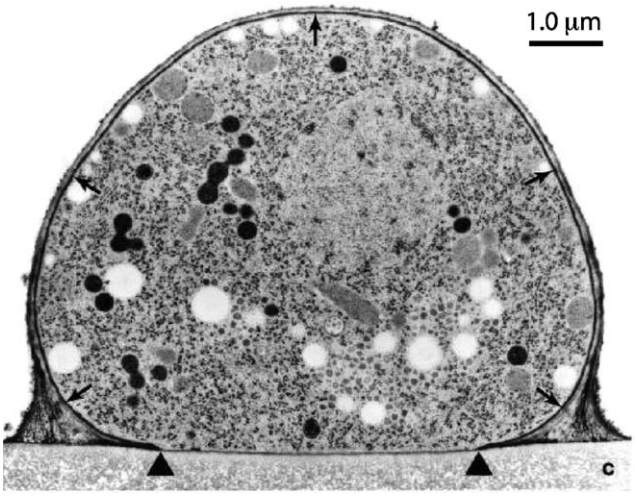

Fig. 2. A typical wild-type appressorial structure prior to peg penetration (reproduced with permission from Howard and Valent (1996)). The two arrowheads at the base of the appressorium indicate the range of the appressorial pore. The dark inner circle, indicated by the small arrows, is the melanin layer. In this image the appressorium is on a cellophane substrate.

glycerol concentration of approximately 3.2 M (DeJong et al., 1997), enormous internal pressures can develop. An electron micrograph of a typical appressorial cross-section is shown in Fig. 2.

6. Experimental evidence (Money and Howard, 1996) indicates at least a threefold increase in turgor pressure after melanization. Other experiments suggest pressures as staggeringly high as 80 atmospheres (Howard et al., 1991). Despite the large increase in pressure there does not appear to be any significant change in the size of the appressorium during this phase.
7. Through pressure, enzymatic degradation, or a combination of both, a penetration peg is blasted through the surface of the rice leaf. The forces involved are so great that, as demonstrated in laboratory experiments (Howard and Ferrari, 1989), the peg can penetrate thin sheets of mylar.
8. The plant cell is invaded with a network of hyphae emanating from the penetration peg. These hyphae eventually break through the leaf surface depositing new conidia and the life cycle is perpetuated.

Although there are many important stages in this life cycle, a critical and intriguing step is the formation and structure of the appressorium, and its ability to withstand such enormous internal pressures. In this paper we concentrate on developing a biomechanical model of the appressorium in order to address two basic questions. The first concerns a determination of the basic appressorial design. This question has a classical engineering counterpart; namely determining the optimal shape of pressurized storage vessels. The second question concerns the extent to which such a structure can withstand the enormous increases in internal pressure that occur after melanization.

2. Basic biomechanical model

We will develop a description of the appressorium in terms of elastic shell theory. In the biological context the use of this framework has been well established for the modeling of red blood cells (Evans and Skalak, 1980; Secomb et al., 1986) and, more recently, used to model hyphal growth in actinomycetes (Goriely and Tabor, 2003a, b). There are many applications of shell theory to problems in engineering (Green and Adkins, 1970; Green and Zerna, 1992) and fluid mechanics (Podgorski and Belmonte, 2004).

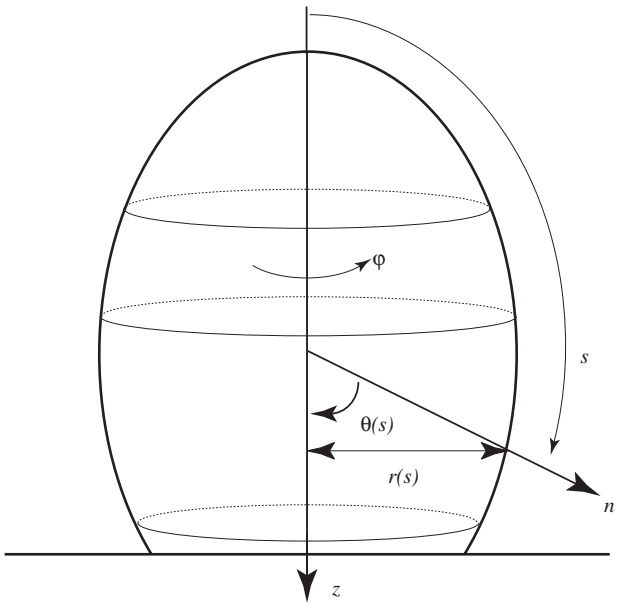

Fig. 3. Basic geometry of the appressorium. The origin of the z-axis is set at the top of the appressorium. Arc-length, s, to a given material point is measured from the top of the shell, $r(s)$ is the radial distance from the vertical axis to that point, and $\mathbf{n}$ denotes the normal direction. The shell is taken to be axisymmetric with azimuthal angle φ.

2.1. Geometry of the problem

The exterior appressorial wall is represented as an elastic shell whose basic geometry is shown in Fig. 3. The shape, which is assumed to be rotationally symmetric about the z-axis, is described in terms of the deformation variables

$$\lambda_s = \frac{\mathrm{d}s}{\mathrm{d}\sigma}, \quad \lambda_\varphi = \frac{r(\sigma)}{r_0(\sigma)}, \tag{1}$$

where s is the arc-length in the deformed configuration and σ is the material coordinate, that is the arc-length of the reference configuration defined by its radius $r_0(\sigma)$. The variables λ_s and λ_φ measure, respectively, the meridional and azimuthal stretches of the shell. For an incompressible shell the third deformation variable, λ_3, measuring changes in the normal thickness of the shell, is simply related to λ_s and λ_φ through the incompressibility condition $\lambda_s\lambda_\varphi\lambda_3 = 1$. The geometric variables satisfy the equations

$$\frac{\mathrm{d}r}{\mathrm{d}s} = \cos(\theta), \tag{2}$$

$$\frac{\mathrm{d}z}{\mathrm{d}s} = -\sin(\theta), \tag{3}$$

and the principal curvatures of the shell are given by

$$\kappa_s = \frac{\mathrm{d}\theta}{\mathrm{d}s}, \tag{4}$$

$$\kappa_\varphi = \frac{\sin\theta}{r}. \tag{5}$$

The sign on the right-hand side of (3) is negative in this model since z is measured from the top of the appressorium.

2.2. Mechanics

The mechanical equilibrium, including bending moments, is governed by the equations (Evans and Skalak, 1980)

$$\frac{1}{r}\frac{\mathrm{d}(rq_s)}{\mathrm{d}s} = \Delta P + \tau_n - (\kappa_s t_s + \kappa_\varphi t_\varphi), \tag{6}$$

$$\frac{1}{r}\frac{\mathrm{d}(rt_s)}{\mathrm{d}s} = \frac{\cos\theta}{r}\, t_\varphi + \kappa_s q_s - \tau_s, \tag{7}$$

$$\frac{1}{r}\frac{\mathrm{d}(rm_s)}{\mathrm{d}s} = \frac{\cos\theta}{r}\, m_\varphi + q_s, \tag{8}$$

where t_s and t_φ are, respectively, the meridional and azimuthal stresses; m_s and m_φ are the bending moments; q_s is the shear force normal to the surface; τ_s is the (external) tangential shear stress acting on the shell; ΔP is the pressure jump between the inside of the membrane and its surrounding, and τ_n is an additional normal stress due to external (normal) forces acting on the membrane different from the pressure jump (in our case, it will be used to model the normal force generated by adhesion to the substrate).

2.3. Constitutive relationship

In order to close the system of mechanical and geometric equations constitutive relations must be introduced. These are developed through the introduction of an elastic free energy function

$$W = W(I_1, I_2, I_3), \tag{9}$$

where I_1, I_2, I_3 are the strain invariants

$$I_1 = \lambda_s^2 + \lambda_\varphi^2 + \lambda_3^2, \tag{10}$$

$$I_2 = \lambda_s^2\lambda_\varphi^2 + \lambda_s^2\lambda_3^2 + \lambda_\varphi^2\lambda_3^2, \tag{11}$$

$$I_3 = \lambda_s\lambda_\varphi\lambda_3. \tag{12}$$

The incompressibility condition implies that both $\lambda_3 = 1/\lambda_s\lambda_\varphi$ and that W does not depend on the third strain invariant, $I_3 = 1$. Standard shell theory (Green and Adkins, 1970) shows that the stresses are given by the relations

$$t_s = 2h\lambda_3(\lambda_s^2 - \lambda_3^2)\left(\frac{\partial W}{\partial I_1} + \lambda_\varphi^2\,\frac{\partial W}{\partial I_2}\right), \tag{13}$$

$$t_\varphi = 2h\lambda_3(\lambda_\varphi^2 - \lambda_3^2)\left(\frac{\partial W}{\partial I_1} + \lambda_s^2\,\frac{\partial W}{\partial I_2}\right), \tag{14}$$

where h is the shell thickness. Using these formulae we note that

$$t_s - t_\varphi = 2h\lambda_3(\lambda_s^2 - \lambda_\varphi^2)\left(\frac{\partial W}{\partial I_1} + \lambda_3^2\,\frac{\partial W}{\partial I_2}\right). \tag{15}$$

The choice of W depends on the problem at hand. The simplest choice is the neo-Hookean model

$$W = C_1(I_1 - 3), \tag{16}$$

where the coefficient C_1 for small deformation is related to Young's modulus by $E = 6C_1$. Nonlinear responses can be captured by considering corrections to the neo-Hookean behavior. A common choice for elastomers is the Mooney–Rivlin model

$$W = C_1[(I_1 - 3) + \mu(I_2 - 3)]. \tag{17}$$

Given any model, we write the constitutive relationships (13), (14) in the form

$$t_s = Af_s(\lambda_s, \lambda_\varphi), \tag{18}$$

$$t_\varphi = Af_\varphi(\lambda_s, \lambda_\varphi), \tag{19}$$

where f_s, f_φ are dimensionless functions and $A = 2hC_1$ provides the dimensional factor appropriate for the subsequent discussion of the scaling of the equilibrium equations. For small deformations the neo-Hookean model gives constitutive relations similar to those of standard linear elasticity theory and it is sometimes convenient to refer (albeit imprecisely) to these relations as "linear". As will be seen below a neo-Hookean type model is adequate to explain the basic appressorial shape, but not to explain the behavior under high pressures.

Finally, we need to specify a constitutive relationships for the bending moments. The bending moments are assumed to be isotropic and proportional to the change in the surface's mean curvature, i.e.

$$m_\varphi = m_s = B(\kappa_s + \kappa_\varphi - K_0), \tag{20}$$

where K_0 is the initial mean curvature and B is the bending modulus (Evans and Skalak, 1980; Secomb et al., 1986).

2.4. Shell equations

The geometric and mechanical equations can be combined to give a closed system. It is convenient to express all the derivatives in terms of the material coordinate, σ, leading to

$$\frac{\mathrm{d}z}{\mathrm{d}\sigma} = -\lambda_s \sin(\theta), \tag{21}$$

$$\frac{\mathrm{d}r}{\mathrm{d}\sigma} = \lambda_s \cos(\theta), \tag{22}$$

$$\frac{\mathrm{d}\theta}{\mathrm{d}\sigma} = \lambda_s \kappa_s, \tag{23}$$

$$\frac{\mathrm{d}\kappa_s}{\mathrm{d}\sigma} = \lambda_s \left[\frac{\cos\theta}{r}\left(\frac{\sin\theta}{r} - \kappa_s\right) + \frac{q_s}{B}\right], \tag{24}$$

$$\frac{\mathrm{d}t_s}{\mathrm{d}s} = \lambda_s \left[A\,\frac{\cos\theta}{r}(f_\varphi - f_s) + \kappa_s q_s - \tau_s\right], \tag{25}$$

$$\frac{\mathrm{d}q_s}{\mathrm{d}\sigma} = \lambda_s \left[\Delta P + \tau_n - \kappa_s t_s - \frac{\sin\theta}{r}\,t_\varphi - q_s\,\frac{\cos\theta}{r}\right], \tag{26}$$

where (24) is obtained from (8) using the constitutive relation (20) and Eq. (5) is used to express κ_φ in terms of r and θ. In Eqs. (25) and (26) t_s and t_φ are expressed in terms of λ_s and λ_φ through the constitutive relations (18), (19), and Eq. (25) is converted into a differential equation for λ_s by eliminating λ_φ through the relation $\lambda_\varphi = r/r_0$.

The six ordinary differential equations (21)–(26) together with the relationships (18), (19) and $\lambda_\varphi = r/r_0$ form a closed system for the variables $(z, r, \theta, \kappa_s, \lambda_s, q_s)$ that can be solved for given initial profile $r_0(s)$, elastic parameters A, B, pressure jump ΔP, external stresses τ_s, τ_n, and appropriate boundary values (see below).

2.5. Membrane limit

In the study given below we will investigate the effect of bending moments. In those cases where they are found to play a relatively minor role they can be neglected and the shell no longer supports an out-of-plane shear force, i.e. $q_s = 0$. Eq. (26) reduces to

$$\Delta P' = \kappa_s t_s + \kappa_\varphi t_\varphi, \tag{27}$$

which is just a generalized form of the Young–Laplace law (where we have set $\Delta P' = \Delta P + \tau_n$). The overall system of shell equations reduces to

$$\frac{\mathrm{d}z}{\mathrm{d}\sigma} = -\lambda_s \sin(\theta), \tag{28}$$

$$\frac{\mathrm{d}r}{\mathrm{d}\sigma} = \lambda_s \cos(\theta), \tag{29}$$

$$\frac{\mathrm{d}\theta}{\mathrm{d}\sigma} = \lambda_s \kappa_s, \tag{30}$$

$$\frac{\mathrm{d}\kappa_s}{\mathrm{d}\sigma} = \lambda_s \left[\frac{\cos\theta}{r}\left(\frac{\sin\theta}{r} - \kappa_s\right)\right], \tag{31}$$

$$\frac{\mathrm{d}t_s}{\mathrm{d}s} = \lambda_s \left[\frac{A\,\cos\theta}{r}(f_\varphi - f_s) - \tau_s\right]. \tag{32}$$

Again, using the constitutive relationship $t_s = A f_s(\lambda_s, r/r_0)$, we obtain a closed system of five equations for $(z, r, \theta, \kappa_s, \lambda_s)$ with initial profile $r_0(s)$, tangential shear τ_s, and boundary values.

2.6. Scaling

First we look at a dimensionless form of the equation and then discuss relevant length scales for the problem. The stresses $t_s, t_\varphi, \tau_s, \tau_n$ and elastic parameter A all have the dimensions of a force per unit length, whereas the pressure is force per unit area. We can rewrite the equations in dimensionless form by expressing all lengths as a multiple of a typical length scale l_0, and by introducing the dimensionless parameter

$$\Gamma = \frac{l_0 \Delta P}{A}, \tag{33}$$

where ΔP is the (constant) pressure difference across the membrane. The number Γ controls the shape of the shell or membrane and expresses the relative effect of pressure difference versus rigidity. That is, a twofold increase in pressure corresponds to a doubling of the parameter Γ, while the same shape can be obtained if both pressure and rigidity change so that their ratio is constant.

Here we choose the characteristic length scale l_0 to be of the order of the observed appressorial radius (see Fig. 2), namely

$$l_0 \sim 3\,\mu\mathrm{m}. \tag{34}$$

Experimental data (Money and Howard, 1996; Howard et al., 1991; DeJong et al., 1997; Howard and Ferrari, 1989; Howard and Valent, 1996) indicate a typical range for the turgor pressure of $\Delta P \sim 1$–$8\,\mathrm{MPa}$, and the overall thickness of the shell is estimated to be $h \sim 0.1\,\mu\mathrm{m}$. Young's modulus E is estimated by using the Young–Laplace law, leading to $E \sim 10$–$100\,\mathrm{MPa}$, which corresponds to $A \sim 1$–$10\,\mathrm{N\,m^{-1}}$. This type of estimate has been shown to be valid for quite a large class of microorganisms by Boudaoud (2003) who investigates a variety of scaling laws for the size of these organisms. Our estimate of E is also consistent with that of many other biological materials as shown in the elastic

moduli atlases of Ashby et al. (1995). Our choice of scales leads to a value of Γ of order unity which will be the reference point for our numerical studies. From now on the governing equations will be solved in dimensionless form and various effects will be discussed as different parameters are changed.

3. Appressorial design

Our first task is to consider the initial appressorial design from a biomechanical perspective. The goal is to determine the extent to which mechanical factors, such as pressure, bending moments, gluing forces, etc., can influence the design and result in a shape as shown in Fig. 2. The appressorium will be modeled as an axisymmetric, incompressible, elastic shell glued to a solid base (the rice leaf) subject to turgor pressure and the adhesive force of the glue. The microscopic scale of the appressorium means that gravitational forces are negligible.

Detailed modeling of the adhesive force is nontrivial and here we employ a very simple heuristic approach in which the glue exerts a downward, spring-like, force between the shell and the leaf surface proportional to the glue-layer thickness at each point (Fig. 4). The glueing force is expressed as

$$\mathbf{g} = -\alpha z \mathbf{e}_z, \tag{35}$$

where α is a phenomenological glueing "strength" parameter, z is the vertical thickness of the glue layer at each point, and $\mathbf{e}_z$ is the vertical unit vector. The glueing force is resolved into normal, g_n, and tangential, g_s, components. The net effect of g_n is a phenomenological increase of pressure in the shell in the glueing region taken into account by identifying g_n with τ_n, while g_s plays the role of τ_s in Eq. (25). We comment that other representations of the glueing force are also possible, such as simply choosing $\mathbf{g}$ to be constant. Another parameter is needed to characterize the glue ring, namely its size. Examination of the experimental pictures, such as those shown in Fig. 2, suggests a characterization in terms of the (apparent) arc-length of the appressorium to which the glue ring is attached. Thus we introduce a parameter η representing this quantity in terms of a percentage of the total arc-length from the base of the appressorium to its top. For example a value of $\eta = 0.1$ means that the lower 10% of the initial appressorium configuration is glued to the base. The beginning of the glue ring is taken to coincide with the end-point of the numerical boundary value problem (in effect corresponding to the edge of the appressorial pore). Therefore, if L is the initial arc-length of the profile, and in the absence of other external stresses, we can make the identification

$$(\tau_s, \tau_n) = \begin{cases} 0 & \text{for } 0 \leqslant \sigma \leqslant (1-\eta)L, \\ (g_s, g_n) & \text{otherwise,} \end{cases} \tag{36}$$

where we recall that distance is measured from the top of the appressorium.

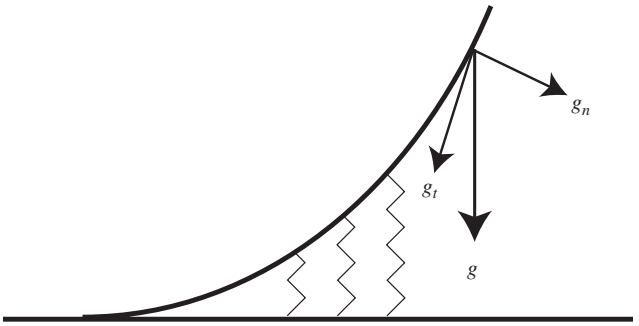

Fig. 4. The glue is modeled as a downward, spring-like, force connecting the shell to the leaf surface. The glueing force $\mathbf{g}$ is assumed proportional to the thickness of the glue at each point and is resolved into normal, g_n, and tangential, g_s, components.

4. Analysis at regular pressure

We now display a series of calculations of the appressorium as a function of the parameters at our disposal for the value of $\Gamma = 1$ that we take to correspond to the appressorial phase before there is any significant increase in turgor pressure and peg-penetration (i.e. in a relatively low turgor pressure regime). We begin by considering the basic appressorial shape in this regime as determined by a Mooney–Rivlin free energy function (17) in the absence of bending moments. For the glueing parameters $\alpha = 1$, $\eta = 0.25$, we show in Fig. 5 the appressorial shapes as a function of the elastic parameter μ. Two features of these computations are immediately apparent: (i) that the shape is already strikingly close to the observed shapes as illustrated in Fig. 2, and (ii) that it is not especially sensitive to the value of μ. Since we currently have no way of estimating μ experimentally, these calculations support the choice of $\mu = 0$ which corresponds to a neo-Hookean material. At a numerical level, a small value of μ increases the convergence of boundary value

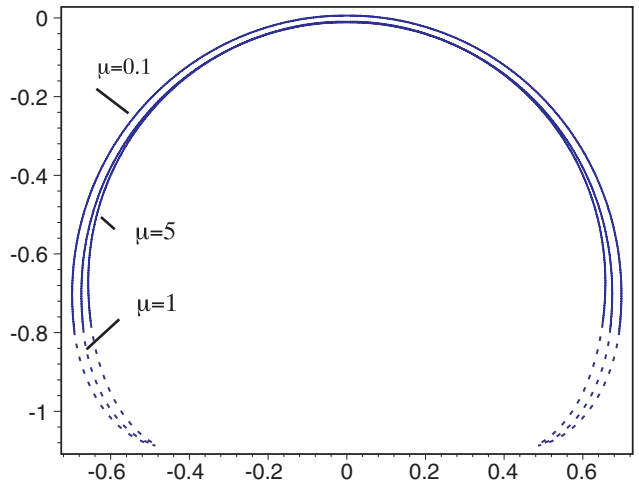

Fig. 5. Appressorial shape for $\Gamma = 1$, $\alpha = 3$, $\eta = 0.25$, and $\mu = 0.1, 1, 5$. The dashed portion of the curve corresponds to the portion of the shell glued to the leaf surface.

problem solvers when large values of Γ are used (see Fig. 9). Therefore, unless explicitly noted we adopt the neo-Hookean material for the remaining calculations.

We now examine, for fixed Γ, the effects of glue ring strength and glue ring size. In Fig. 6 we show the shell shapes for different glue ring sizes for a fixed glue strength; and for different glue strengths for a fixed ring size. Overall, the trend is clear: as the glue ring size and glue strength are increased the base of the appressorium bulges down towards the leaf surface.

The increased bending at the base of the shell that occurs with increased glue strength and ring size suggests that bending moments might be important. In Fig. 7 we show the effect of including these moments for varying values of the bending modulus B. The larger the bending modulus, the greater the resistance to bending—leading to more elongated shapes, while for smaller B values the shell shapes exhibit greater curvature.

In order to compare the computed shapes with the experimental observations we superimpose the case of a typical shell-shape, computed with bending moments, over Fig. 2. The agreement, as shown in Fig. 8 is quite striking. Furthermore, the calculations described above indicate that, overall, the appressorial shape is rather robust with respect to the various parameters that can influence it.

The results also indicate that while the inclusion of small bending effects modifies the shell shapes somewhat they do not lead to any dramatic changes and in the remaining computations bending moments are neglected unless otherwise stated.

The observed dome-like shape is consistent with storage vessel shapes that can be found in the classical engineering literature (see, for example, Timoshenko, 1940, Fig. 147). In this classical case, the shape depends on the force exerted by the heavy liquid in the tank. At the microscopic level gravitational effects are negligible but the glueing force plays, effectively, an analogous role in shaping the appressorial dome.

5. Appressorial response to increased pressure

All the above calculations pertain to the shape of the appressorium in a relatively early phase, well before the occurrence of peg penetration, when the turgor pressure is relatively low (although in the above comparison with experiment melanization has occurred). As discussed earlier, the experimental results show that after the melanin layer has formed very large turgor pressures can eventually develop and, furthermore, that there is apparently no significant increase in the appressorial shape when this

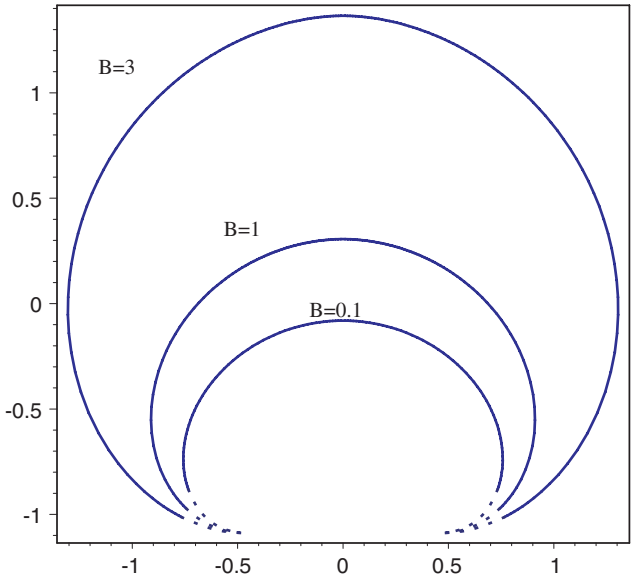

Fig. 7. Appressorial shapes with $\Gamma = 1$, $\mu = 0$, $\alpha = 3$, $\eta = 0.25$ for different values of the bending modulus, $B = 0.1, 1, 3$.

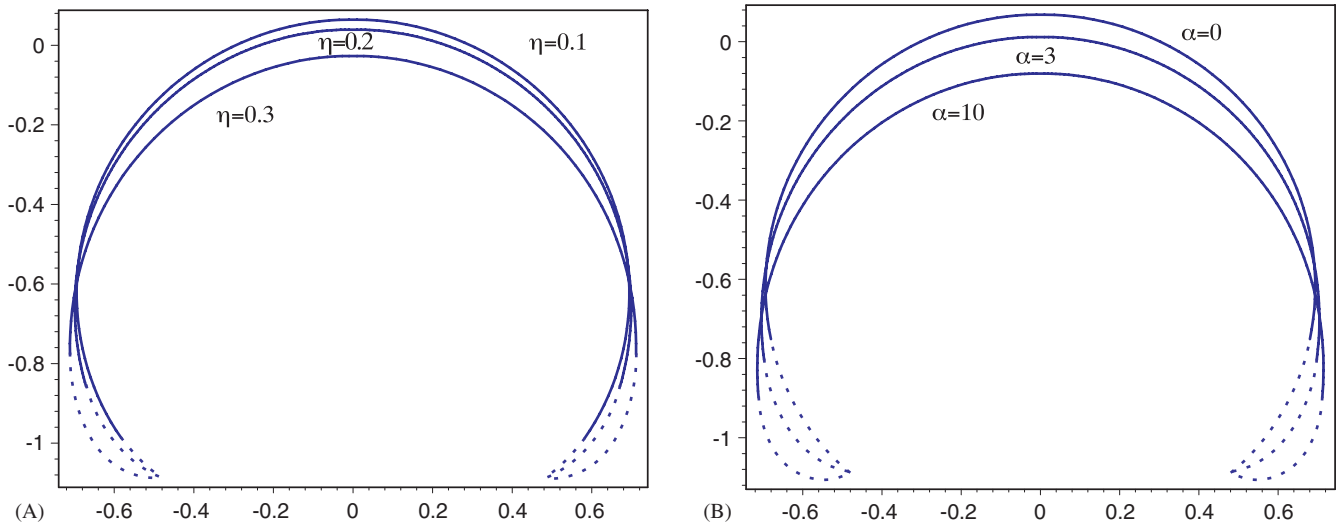

Fig. 6. (A) Appressorial shapes with $\Gamma = 1$, $\mu = 0$, $\alpha = 3$, and ring sizes of $\eta = 0.05, 0.20, 0.30$. The dashed portion of the curve corresponds to the portion of the shell glued to the leaf surface. (B) Shapes for $\Gamma = 1$, $\mu = 0$, $\eta = 0.25$, and $\alpha = 0, 3, 10$.

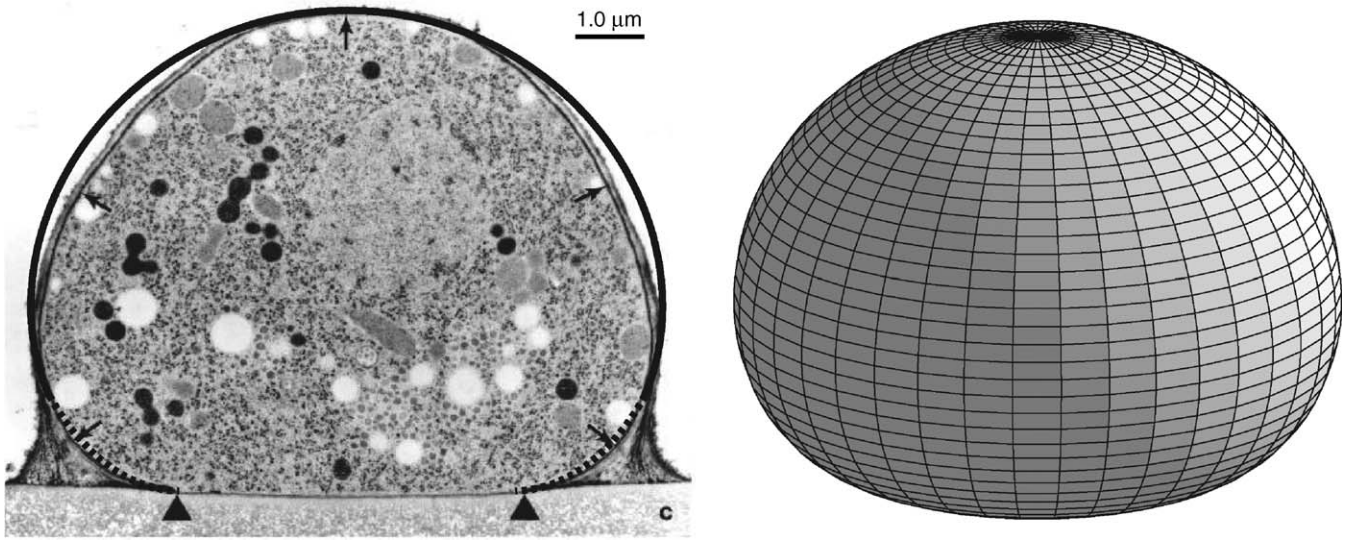

Fig. 8. Computed appressorial shape (heavy line) with $\Gamma = 1$, $\mu = 0$, $\alpha = 3$, $\eta = 0.20$, compared with Fig. 2. The dashed line represents the glued portion of the appressorium. The calculation includes bending moments ($B = 0.10$). The plot on the left is the 3-dimensional version of the numerical solution.

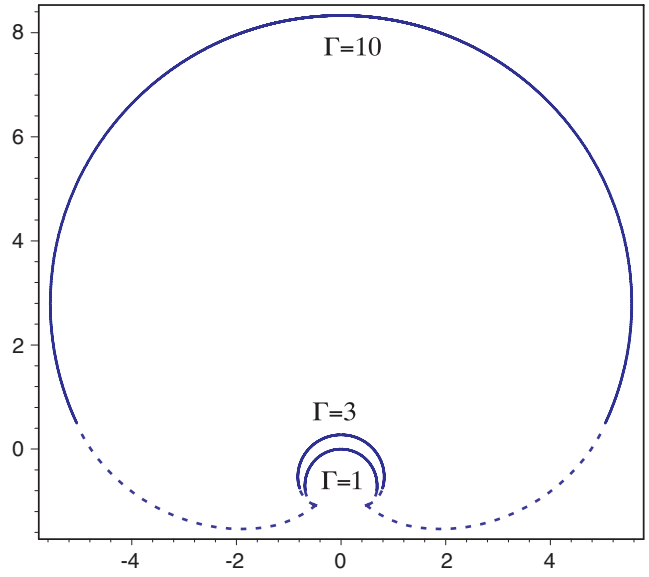

Fig. 9. Initial appressorial shape $\Gamma = 1$, $\mu = 0.3$, $\alpha = 3$, $\eta = 0.25$ subjected to increased effective pressure $\Gamma = 3$ and $\Gamma = 10$. A small value of the nonlinear coefficient μ in the Mooney–Rivlin free energy has been used for these simulations to stabilize the computations for large Γ values.

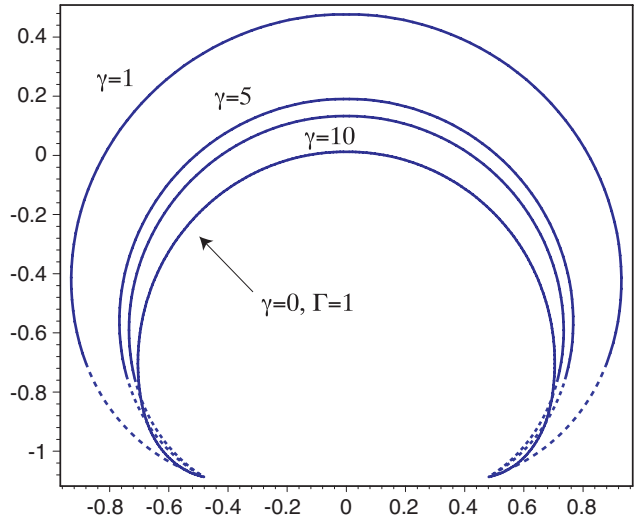

Fig. 10. Appressorial shapes with $\Gamma = 10$, $\alpha = 3$, $\eta = 0.25$ with varying nonlinearity $\gamma = 1, 5, 10$. The innermost curve corresponds to the shell shape computed with the neo-Hookean free energy with $\Gamma = 1$.

occurs. This later observation is intriguing from the mechanical point of view. To investigate this we take a shell calculation, using a neo-Hookean elastic energy, with typical parameters and effective pressure $\Gamma = 1$ as the reference configuration, and then increase Γ threefold and tenfold. As shown in Fig. 9 a threefold increase in effective pressure leads to a relatively modest increase in appressorial dimension (about a 10% increase in height) whereas a tenfold increase, which is apparently possible according to some experimental data, leads to a very substantial swelling of the appressorium. Since this order of size increase is apparently not observed, this suggests a "failure" of the current model. We believe that the problem simply lies in the nature of the constitutive relations which, in the case of the neo-Hookean or Mooney–Rivlin models, are not suitable for appressorial wall material—which clearly shows considerable rigidity under high stresses. This can be modeled by choosing an elastic free energy yielding highly nonlinear constitutive relations able to reflect this behavior. One possible choice is the Fung model (1993) which takes the form

$$W = \frac{C_1}{\gamma}(e^{\gamma(I_1-3)} - 1) \tag{37}$$

which, in the limit $\gamma \to 0$ (or for small enough values of the invariant), reduces to the neo-Hookean model. Fig. 10 shows the behavior of a shell modeled with the Fung free energy, with an effective pressure of $\Gamma = 10$, for different values of the rigidity parameter γ. The results clearly show that with increasing values of this parameter the shell is evermore resistant to expansion, even under high pressure.

6. Results and discussion

By modeling the appressorial wall as an elastic shell subject to turgor pressure and employing a simple representation of adhesive forces, we have been able to show that the basic design of the appressorium is robustly consistent with mechanical principles. One of the striking features of the appressorial design is its ability to withstand enormous increases in turgor pressure with apparently little change in shape. This behavior appears to be well modeled by employing a nonlinear constitutive relationship reflecting an increasing rigidity of the shell wall under high stresses.

Acknowledgements

This work is supported by the NSF Grant DMS-0307427. A.T. acknowledges partial fellowship support from NSF IGERT Grant NSF DGE-9870659. The authors thank N.P. Money for a number of very helpful conversations and comments on the manuscript, R.J. Howard for permission to reproduce Fig. 2 and other communications, Marc Orbach and his research group for helpful discussions and access to their laboratory data, and Dave Bentley (Arizona Research Laboratories Imaging Facility) for help with some data analysis. The authors also thank Arezki Boudaoud and Axel Buguin for valuable discussions.

References

Ashby, M.F., Gibson, L.J., Wegst, U., Olive, R., 1995. The mechanical properties of natural materials. I. Material property charts. Proc. R. Soc. Lond. A 450, 123–140.

Bastmeyer, M., Deising, H.B., Bechinger, C., 2002. Force exertion in fungal infection. Annu. Rev. Biophys. Biomol. 31, 321–341.

Boudaoud, A., 2003. Growth of walled cells: From shells to vesicles. Phys. Rev. letts. 91, 018104-1–018104–4.

DeJong, J.C., McCormack, B.J., Smirnoff, N., Talbot, N.M., 1997. Glycerol generates turgor in rice blast. Nature 389, 244–245.

Evans, E.A., Skalak, R., 1980. Mechanics and Thermodynamics of Biomembranes. CRC Press, Boca Raton, FL.

Fung, Y.C., 1993. Biomechanics: Material Properties of Living Tissues. Springer, New York.

Goriely, A., Tabor, M., 2003a. Biomechanical models of hyphal growth in actinomycetes. J. Theor. Biol. 222 (2), 211–218.

Goriely, A., Tabor, M., 2003b. Self-similar tip growth in filamentary organisms. Phys. Rev. Lett. 90 (10), 108101-1–108101-4.

Green, A.E., Adkins, J.E., 1970. Large Elastic Deformations. Clarendon Press, Oxford.

Green, A.E., Zerna, W., 1992. Theoretical Elasticity. Dover Publications, New York.

Howard, R.J., Ferrari, M.A., 1989. Role of melanin in appressorium function. Exp. Mycol. 13, 403–418.

Howard, R.J., Valent, B., 1996. Breaking and entering: host penetration by the fungal rice blast pathogen *Magnaporthe grisea*. Annu. Rev. Microbiol. 50, 491–512.

Howard, R.J., Ferrari, M.A., Roach, D.H., Money, N.P., 1991. Penetration of hard substrates by a fungus employing enormous turgor pressures. Proc. Natl Acad. Sci. USA 88, 11281–11284.

Money, N.P., Howard, R.J., 1996. Confirmation of a link between fungal pigmentation, turgor pressure, and pathogenicity using a new method of turgor measurement. Fungal Genet. Biol. 20, 217–227.

Podgorski, R., Belmonte, A., 2004. Surface folding of viscoelastic fluids: finite elasticity membrane model. European Journal of Applied Mathematics 15, 385–408.

Secomb, T.W., Skalak, R., Ozkaya, N., Gross, J.F., 1986. Flow of axisymmetric red blood cells in narrow capillaries. J. Fluid Mech. 163, 405–423.

Talbot, N.J., 2003. On the trail of a cereal killer: exploring the biology of *Magnaporthe grisea*. Annu. Rev. Microbiol. 57, 177–202.

Timoshenko, S., 1940. Theory of Plates and Shells. McGraw-Hill Book Company, New York, London.